IEEE Access
Multidisciplinary | Rapid Review | Open Access Journal

Received December 1, 2020, accepted January 1, 2021, date of publication January 8, 2021, date of current version January 21, 2021.

Digital Object Identifier 10.1109/ACCESS.2021.3050260

Image Haze Removal Algorithm Using a Logarithmic Guide Filtering and Multi-Channel Prior

YUANYANG ZOU[1], YINGSHUANG MA[2], LIYUN ZHUANG[3], AND GUOXIN WANG[4]

[1]School of Business Administration, Hubei University of Economics, Wuhan 430205, China
[2]Business College, Huanggang Normal University, Huanggang 438000, China
[3]Faculty of Electronic Information Engineering, Huaiyin Institute of Technology, Huaian 223003, China
[4]School of Mathematics and Physics, Nanyang Institute of Technology, Nanyang 473004, China

Corresponding author: Liyun Zhuang (zlytpjs@hyit.edu.cn)

This work was supported in part by the Natural Science Foundation of China under Grant 11901320.

ABSTRACT In reality, the quality of an image is generally affected by haze. To obtain a well-quality image, removing haze is a hot issue on theory and application. This paper proposes a new algorithm to remove haze of hazy images. In the algorithm, first, the ambient illumination is estimated by a logarithmic guide filtering that can reserve the characteristics of the bright source areas and improve the dark source areas of the hazy image. Second, to overcome the defect of dark channel prior (DCP) and the over-brightness of the bright channel prior (BCP), two models with two parameters are introduced to improve the DCP and BCP, called multi-channel prior method. At the same time, a self-adaptive method is presented to compute the values of the two parameters. At last, based on the multi-channel prior, a self-adaptive method is proposed to compute the transmission mapping value. Further, four classes hazy images are employed to test the proposed method. The experimental results carried out on the public databases demonstrate that the proposed algorithm can outperform the current state-of-the-arts, including more effective defogging, clearer visibility and richer details.

INDEX TERMS Remove haze, hazy image, logarithmic guide filtering, multi-channel prior.

I. INTRODUCTION

Due to the fact that the haze or fog affects the ambient illumination, a hazy or foggy image is usually captured by camera or video. Zhang *et al.* [1] stated that the haze or fog can lead to the challenge of the monitoring equipment in the foggy or hazy environment such as topographic surveillance, outdoor reconnaissance and intelligent traffic. Thus, hazy- or foggy-free is a significant issue being energetically handled by scholars. In all, two aspects should be considered: estimating the ambient illumination of the hazy or foggy image and handling the light source regions.

Generally, the ambient illumination is affected by fog, water vapours or dust. Thus, removing the haze or fog of an image, the ambient illumination should be considered. Laine [2] studied that the ambient illumination affected on the observed color of an image, who stated that the ambient illumination was affected by perceived color on an awning. Moreover, that the influence of ambient illumination on the diagnosis of radiological images was investigated by Brennan *et al.* [3] and Lin and Huang [4]. The effect of ambient light on the comprehension for characters presented on a screen was presented by Gong *et al.* [5]. Therefore, how to precisely estimate the ambient illumination is a key problem in the image processing. Many related works of the ambient illumination estimating are proposed in the image processing area [6]–[9].

Further, the dark channel prior (DCP) is a popular method to deal with the generally hazy image [10]. The performance of the DCP approach is poor for heavy hazy images and the processed image looks dark. Thus, how to handle the light source regions is also an important problem of the heavy hazy image.

This paper proposes a novel method for the heavy hazy and light hazy images. In the proposed method, ambient illumination is estimated by a non-linear algorithm. The contributions are:

The associate editor coordinating the review of this manuscript and approving it for publication was Yudong Zhang.

- First, this paper proposes a logarithmic guide filtering to predict the ambient illumination, which can retain the smooth of the image as well as reservable edges of different areas of the image and substitute of employing the input image for estimating ambient illumination.
- Second, multi-block bright channel prior approach, in which two parameters are introduced to overcome the fault of the DCP and bright channel prior (BCP) and are estimated by an adaptive method, is employed to deal with dark source areas and light source areas in the algorithm.
- At last, combining with the multi-block bright channel prior method, an adaptive method is stated to calculate the transmission factor.

The remainder of this paper is organized as follows: The related works of this paper are discussed in Section 2; The proposed method is described in Section 3. In Section 4, light and heavy hazy images are utilized to test our method, and the experimental results and discussion are presented. The conclusions of this investigation are drawn in Section 5.

II. RELATED WORK

One of the main method for dehazing images is to decrease the fog or haze of the hazy or foggy images. Koschmieder [11] firstly stated the physical model to improve the quality of a foggy image.

$$I(x) = t(x)J(x) + (1 - t(x))A, \tag{1}$$

where $I(x) = (I^R(x), I^G(x), I^B(x))$ stands for the foggy or hazy image; $J(x)$ is a foggy- or hazy-free image; the atmospheric light is described by constant A. $t(x)(1 < t(x) < 1)$ is a weight factor with respect to the depth of each pixel denoted by x. x stand for the value of the pixel of the hazy image. In equation (1), the airlight is expressed by $(1 - t(x))A$. Based on equation (1), it is easy to obtain the following equation:

$$J(x) = \frac{I(x) - A}{t(x)} + A, \tag{2}$$

called dark channel prior (DCP) algorithm. This method assumed that the surrounded pixel of each pixel must embrace no less than one low-intensity pixel in the colour channel, and it was studied by He *et al.* [12].

Thus, the researches of the general dehazing image are summarized as three categories: prior-based information approaches, machine learning approaches, and multi-scale fusion approaches.

The precondition of the prior-based information algorithms is that the depth-information of input image is necessitated. From this ideal, the prior-based information algorithms stemming from the atmospheric scattering algorithm were stated by Narasimhan and Nayar [13]. Since the depth-information was required in the algorithm, which may lead the algorithm to possession of high computational complicity. Thus, for single image dehazing, different kinds of algorithms were presented. Fattal [14] presented a method to predict the optical transmittal in hazy circumstances, enhance the visual, and recuperate the contrast of haze-free images. The visibility of the bad weather image was studied by Tan [15], who utilized the Markov random variation theory to remove the haze for a hazy image. Nishino *et al.* [16] and Tarel and Hautiere [17] stated algorithms to raise the efficiency and quality of DCP. To signify the spectacle depth of hazy images, a linear algorithm based on a color attenuation prior was proposed by Zhu *et al.* [18], and a supervised method was utilized to obtain the parameters of the algorithm. Fattal [19] revealed that one-dimensional distribution can be employed to express the pixels of image patches and recuperate the spectacle transmission map. Further, more researches of the prior-based information approaches can be found in references [20]–[25].

However, the default of the precondition is still required. Therefore, machine learning approaches are utilized to remove the haze of hazy images. Further, in view of the number of the models, the machine learning approaches can be separated into two types: single-model optimization and combinational-model optimization. Only one of the major factors is handled in the former optimization methods. For replacing the guided image filtering [26], Tang *et al.* [27] presented a learning framework to learn the different haze characteristics for defogging the hazy image. The medium transmission was estimated by the hazy images in a machine learning system, called DehazeNet, which was stated by Cai*et al.* [28]. Based on convolutional neural network, a new image dehazing system, called AOD-Net, was constructed by Li *et al.* [29], which was based on atmospheric light model in [11]. Further, more researches of this type please see [30]–[34]. However, the other factors also generally affect the haze-free quality of the dehazing images such as global atmospheric light. Thus, more factors are considered in the later algorithms. An end-to-end single haze-free algorithm, called Densely Connected Pyramid Dehazing Network (DCPDN), was presented by Zhang and Patel [35]. In the algorithm, the transmission function and atmospheric light were considered together. At the same year, Zhang *et al.* [1] stated a perceptual pyramid deep network algorithm to remove haze of hazy images. The attenuated scene radiance and the atmospheric light were considered in the algorithm. To deal with the dependency of the transmission mapping and atmospheric light, another end-to-end network, called Cycle-Dehaze, was introduced by Engin *et al.* [36], which was utilized to remove haze of the hazy images. Proximal Dehaze-Net [37] was a deep architecture for defogging the hazy image. In some conditions, it is difficult to obtain a high-quality dehazing effect. Some other researches relating the combinational-model optimization approaches were studied in [38]–[43]. In view of the machine learning methods for removing haze of hazy images, first, the machine learning models need to be trained. In this step, the values of parameters in the models are requested to accurately approximate the atmospheric scattering. Then, the haze of hazy images is removed by the machine learning methods with the parameters values obtained by the training step. It is obvious that the values of parameters in the models are not proper for some

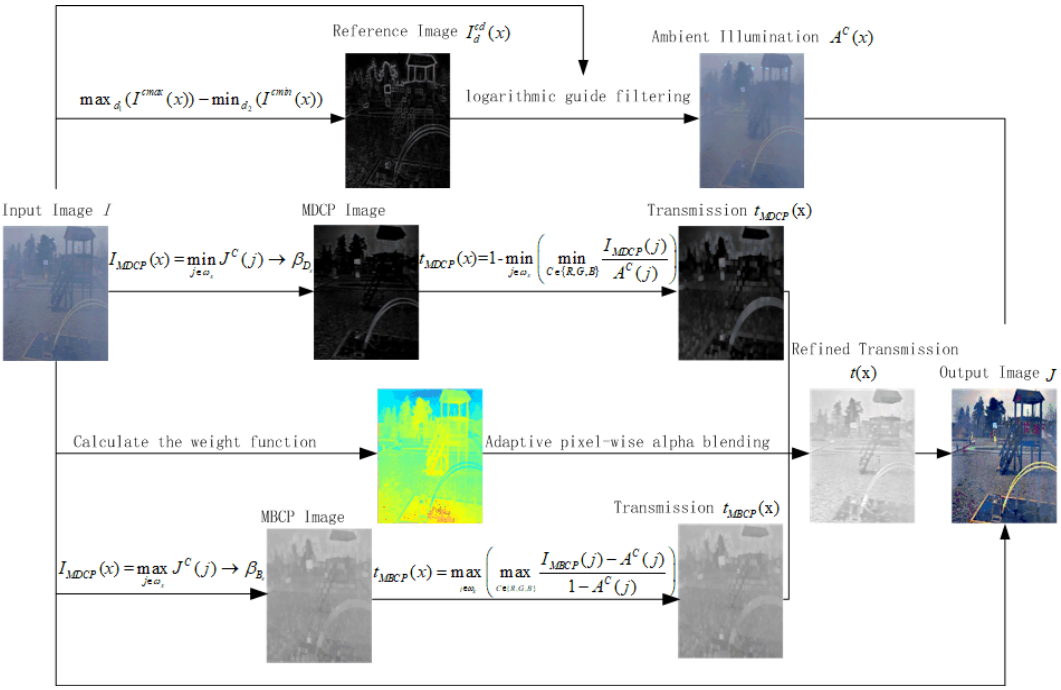

FIGURE 1. Flow chart of the proposed dehazing method.

hazy images, especially when the characteristics between the training hazy images and the testing hazy images are distinguished significantly. The machine learning methods may be not of appositeness.

For addressing the problem which generates from the machine learning methods, multi-scale fusion approaches have been stated into removing haze of hazy images. The first method of the class was stated by Ancuti and Ancuti [44]. In the method, two imported images, which were handled by a white equilibrium and a contrast-enhancing technique, were fused by two corresponding procedures with a multi-scale scheme. In addition, Laplacian pyramid representation was utilized in the study. Since the inadequate blending objects and the imprecise comprehensive atmospheric light, the visuosensory of the method was insufficient. A new fusion method, called FVID (Fusion-based Variational Image-Dehazing), was proposed by Galdran *et al.* [45]. In the method, an optimization model was considered, the objective was utilized to minimize the two energy functions, and a fusion scheme for removing hazy of hazy image. For keeping away the intrusion of the comprehensive atmospheric light, a new method for removing haze of hazy image was introduced by Gao *et al.* [46]. This algorithm used the sky region in place of the whole image to predict the global atmospheric light and amalgamate all the input images which lead to raising the time-depleting. Further, to improve the visual dehazing images and avoid interference factors, the artificial gamma correction, a multi-scale Laplacian pyramid and Gaussian pyramid were utilized into the multi-scale fusion algorithm proposed by Galdran [47], called AMEF. Moreover, other researches of the type, please see [48]–[54]. In addition, to enhance an image, a model-assisted multiband fusion (MAMF) method was proposed by Cho *et al.* [55]. To address the nighttime single foggy image, a pixel-wise alpha blending (PWAB) approach is proposed by Yu *et al.* [56].

In all, all the above researches, to predict the ambient illumination, assumed that the characteristics of ambient illumination of the brightest pixels in local regions of a hazy image can be easily obtained. In view of this assumption, the local regions are white and the transmission value is 0. In addition, the classic DCP is inapplicable for the bright source areas. Thus, in this study, a logarithmic guide filtering is introduced to predict the ambient illumination. Further, two parameters, in which the values of the parameters are adaptively obtained, are introduced to adjust the DCP and BCP. Last, it is also an adaptive method to compute the weight factor in this study.

III. PROPOSED DEHAZING METHOD

As displayed in Figure 1, to remove haze for hazy images, the key steps are addressed in this section.

A. AMBIENT ILLUMINATION ESTIMATION

In view of the depiction of Section 2, atmospheric scattering model (equation (1)) is extensively utilized for removing haze of hazy images. In the model, ambient illumination A is a constant. However, sometimes, the ambient illumination is not a constant especially in the heavy haze situation. That is, the ambient illumination of hazy scenes mainly depend on the values of local extension of pixels. In addition, if the transmission mapping is proximate to 0, the ambient illumination

$A(x)$ is close to the values of the hazy pixel $I(x)$. Land [57] stated that the reflect wavelength determined the color of the object. In other words, different color objects reflect different wavelength. Thus, non-uniform illumination is noneffective for the color of the object. Based on the theory of retinex, observable brightness of an object relays on the ambient illumination and the target surface's reflection. Theoretically, the clear image $J(x)$ can be expressed as two product items. Thus, let $Q(x)$ be the reflection of a target. Then, $J(x)$ can be formulated as

$$J(x) = A(x)Q(x). \tag{3}$$

Then, the atmospheric scattering model (equation (1)) can be rewritten as

$$I(x) = A(x)Q(x)t(x) + A(x)(1 - t(x)). \tag{4}$$

Further, we have

$$I(x) = A(x)(Q(x)t(x) + 1 - t(x)). \tag{5}$$

Obviously, equation (5) is a retinex-like model. In model (5), $A(x)$ can be regarded as a spatially-smooth function for the low frequency areas of a hzay image. Thus, the second item can be regarded as the high frequency areas of a hazy image. Some methods were employed to predict the low frequency item $A(x)$. A low pass filter method was utilized to estimate the low frequency item proposed by Yu *et al.* [58]. In addition, traditional Retinex algorithms with Gaussian filter was employed to predict the low frequency presented in [58]–[60]. Nevertheless, smoothing of all directions of hazy image is isotropic and the edge is not preserved.

In this paper, To address the ambient illumination prediction of a hazy image, a logarithmic guide filtering is proposed. In order to reserve the edges of the hazy image, first, we set forth a channel difference (CD) map to calculate the difference of maximum value and minimum value of each component (R, G, B) of the color hazy image.

$$I_d^{cd}(x) = \max_{d_1}(I^{cmax}(x)) - \min_{d_2}(I^{cmin}(x)). \tag{6}$$

where, d_1 and d_2 are the indexes of the pixel of $x \in \omega_d$; ω_d is a window at the pixel d. Let N denote the number of pixels in the window ω_d. Then, the ambient illumination $A_d(x)$ in the region ω_d can be computed by the following equation (7).

$$A^C(x) = a_d K_N(x) \log I_d^{cd}(x) + b_d, \tag{7}$$

where a_d and b_d are parameters in ω_d. We know that the gradient of logarithmic function is a increasing function. That is, according to the equation, in dark areas, a bigger values of ambient illumination of hazy image can be obtain by equation (7); In bright areas, the ambient illumination should not be changeable or small changeable. Obviously, equation (7) is also satisfiable for this requirement. Then, to obtain the values of parameters a_d and b_d, a smoothing term ηa_d^2 and a cost function are proposed as

$$E(a_d, b_d) = \sum_{x \in \omega_d} (a_d K_N(x) \log I_d^{cd}(x) + b_d - I(x))^2 + \eta a_d^2. \tag{8}$$

where, $K_N(x) = \dfrac{\sqrt{\det(C_N)}}{2\pi\sigma^2} \exp\left\{-\dfrac{(x_p - x_q)^T C_N (x_p - x_q)}{2\sigma^2}\right\}$ is one of the most alluring tools in image processing region proposed by Sun *et al.* [61], called steering kernel. x_p and x_q denote the pixel coordinates. σ is the smoothing parameter, which is utilized to control the supporting range of the kernel. C_N is the covariance matrix calculated of the local square window ω_d centered at pixel d and can be estimated by

$$\begin{aligned} C_N &= \gamma_N U_{\alpha_N} \Lambda_{\sigma_N} U_{\alpha_N}^T, \\ U_{\alpha_N} &= \begin{bmatrix} \cos\alpha_N & \sin\alpha_N \\ -\sin\alpha_N & \cos\alpha_N \end{bmatrix}, \\ \Lambda_{\sigma_N} &= \begin{bmatrix} \sigma_N & 0 \\ 0 & \sigma_N^{-1} \end{bmatrix}, \end{aligned}$$

where γ_N is a constant. U_{α_N} and Λ_{σ_N} are the prolongation matrix by α_N and σ_N respectively. Further, γ_N, α_N, and σ_N are calculated by the single value decomposition (SVD) of the local gradient matrix at pixel d.

In addition, to adaptively obtain the smoothing term, the following equation proposed by Yu *et al.* [58] is utilized.

$$\Psi_N(x) = \frac{1}{N} \sum_{i=1}^{N} \frac{\sigma_{d,1}^2(p) + \varepsilon}{\sigma_{d,2}^2(q) + \varepsilon},$$

where, ε is a very small constant. $\sigma_{d,1}^2(p)$ and $\sigma_{d,1}^2(q)$ are the variance of region ω_d in the 3×3 areas centered at pixels p and q respectively.

Then, equation (8) can be reformulated as

$$\begin{aligned} &E(a_d, b_d) \\ &= \sum_{x \in \omega_d} (a_d K_N(x) \log I_d^{cd}(x) + b_d - I(x))^2 + \frac{\eta}{\Psi_N(x)} a_d^2. \end{aligned} \tag{9}$$

Then, linear ridge regression method can be employed to solve equation (9) and the values of parameters a_d and b_d are expressed as

$$\begin{aligned} a_d &= \frac{\frac{1}{N}\sum_{d \in \omega_d} I_d \log I_d^{cd} - \mu_d \bar{I}_d}{K_N \delta_d^2 + \frac{\eta}{\Psi_N}}, \\ b_d &= \mu_d - a_d K_N \mu_d, \end{aligned} \tag{10}$$

where $\bar{I}_d$ is the average of all pixels in the region ω_d from I_d; μ_d and δ_d are the mean and variance values of all pixels in the region ω_d respectively from I_d. Then, we have

$$A^C(x) = \frac{1}{N} \sum_{d} (a_d K_N(x) \log I_d^{cd}(x) + b_d). \tag{11}$$

B. MULTI-CHANNEL PRIOR

To estimate the transmission $t(x)$, in this section, a multi-channel prior method is presented. In an image, the color characteristics of the bright areas is quite different from those of dark areas. In [12], the dark channel prior method was utilized to handle the dark channel prior. However, the luminance of the image is reduced by DCP method. Thus, in this study, to overcome the fault of the DCP and estimate the dark channel prior, a parameter β_{D_s} is utilized and s is the index of the dark areas in an image, we propose a multi-channel prior method to cope the BCP and DCP of an image, called modified BCP (MBCP) and modified DCP (MDCP). At the same time, to prevent the excessive bright areas of an image, a parameter β_{B_s} of the bright channel prior in an image is introduced in this study. The expressions of the method are as follows:

$$I_{MDCP}(x) = \min_{j\in\omega_x} J^C(j) \rightarrow \beta_{D_s}, \quad C \in \{R,G,B\}\ x \in DR(dark\ \ regions), \tag{12}$$

and

$$I_{MBCP}(x) = \max_{j\in\omega_x} J^C(j) \rightarrow \beta_{B_s}, \quad C \in \{R,G,B\}\ x \in NDR(bright\ \ regions). \tag{13}$$

It is obvious that the proper value of the parameters in equations (12) and (13) is an important issue. Simply, a fixed value can be set in equations (12) and (13). However, this method cannot suit for different kinds of images. Thus, we present an adaptive method to estimate the parameters β_{D_s} and β_{B_s}. The equations can be expressed as follows:

$$\beta_{D_s} = \min\left\{\frac{x_s}{\sqrt{\sum x_s}}\right\}, \quad x_s \in dark\ \ region,$$

$$\beta_{B_s} = \max\left\{\frac{x_s}{\sqrt{\sum x_s}}\right\}, \quad x_s \in bright\ \ region.$$

C. ADAPTIVE PIXEL-WISE ALPHA BLENDING

Combining subsections III-A and III-B, the ambient illumination is estimated in subsection III-A. Thus, the calculation of transmission mapping $t(x)$ is proposed in this subsection.

$$t_{MDCP}(x) = 1 - \min_{j\in\omega_x}\left(\min_{C\in\{R,G,B\}}\frac{I_{MDCP}(j)}{A^C(j)}\right),$$
$$t_{MBCP}(x) = \max_{j\in\omega_x}\left(\max_{C\in\{R,G,B\}}\frac{I_{MBCP}(j) - A^C(j)}{1 - A^C(j)}\right). \tag{14}$$

According to equation (14), the dark source and bright source areas are computed respectively. However, in a region, the transmission $t(x)$ is only one mapping. Thus, in order to obtain the final transmission mapping $t(x)$, a blend method is utilized for addressing $t(x)$.

$$t(x) = \alpha(x)t_{MBCP}(x) + (1-\alpha(x))t_{MDCP}(x). \tag{15}$$

Here, $\alpha(x)$ is the weight factor of the transmission mapping and is computed by

$$\alpha_C(x) = \max_{C\in\{R,G,B\}}(I^C),$$
$$\alpha(x) = \max\left\{\frac{\alpha_R(x)}{\sum_R \alpha_C(x)}, \frac{\alpha_G(x)}{\sum_G \alpha_C(x)}, \frac{\alpha_B(x)}{\sum_B \alpha_C(x)}\right\}, \tag{16}$$

where I^C is the region ω_d.

After that, a well-quality dehazing image can be obtained by subsections III-A, III-B, and III-C.

IV. EXPERIMENTAL RESULTS AND DISCUSSION

In this section, the performance of the proposed method is evaluated in subjective and objective ways. Some testing images (hazy/foggy) are collected for experiments. These images are selected from RTTS, HSTS, SOTS [62], O-HAZE, I-HAZE and DENSE-HAZE [63]–[65] public datasets, which are subjected to poor illumination conditions and non-uniform illumination images. Figure 2 displays some examples of foggy/hazy images. All the experiments are tested in MATLAB R2018a on a PC with 2.4 GHz CPU and 4 GB RAM.

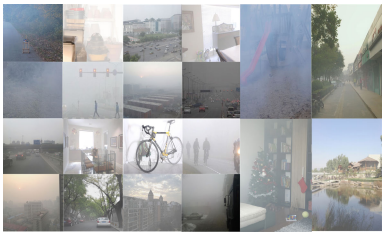

FIGURE 2. Examples of foggy images.

In order to evaluate the effectiveness of the proposed approach, some state-of-the-art technologies are utilized for comparison: DCP [12], Cho *et al.* [55], AMEF[47], Yu *et al.* [56], Cai *et al.* [28] and Yang and Sun [37]. The assessment is performed in subjective and objective ways. To make a fair comparison, the parameters of the selected methods are set according to the suggestions of the authors.

A. SUBJECTIVE EVALUATION

To subjectively evaluate the performance in this section, the testing pictures are named image #1-20, which contain light and heavy haze images. The light haze images (image #1-10) are selected from RTTS, HSTS and SOTS [62], while the heavy haze images (image #11-20) are chosen from O-HAZE, I-HAZE and DENSE-HAZE [63]–[65] public datasets. The selected images can be divided into four types, in which five images are partitioned a type including light haze outdoor (image #1-5), light haze indoor (image #6-10), heavy haze outdoor (image #11-15) and heavy haze indoor (image #16-20).

Figure 3 shows the processed images using various de-fogging methods under light haze outdoor scenarios. The effects of the defogging images are indicated

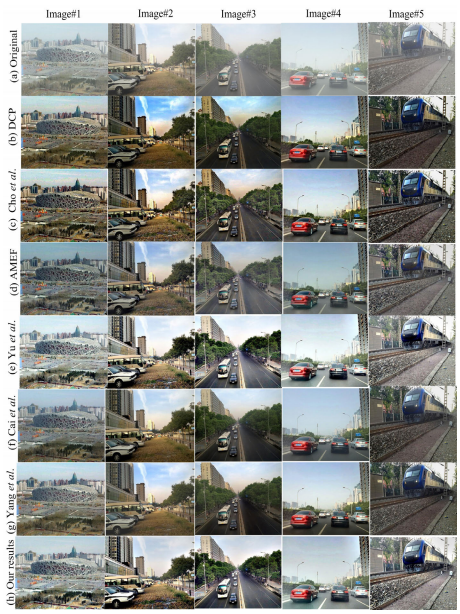

FIGURE 3. Comparisons of light haze outdoor images by various defogging algorithm. (a)Original images. (b)DCP results. (c) Cho *et al.* results. (d) AMEF results. (e) Yu *et al.* results. (f) Cai *et al.* results. (g) Yang *et al.* results. (h) Our results.

FIGURE 4. Comparisons of light haze indoor images by various defogging algorithm. (a)Original images. (b)DCP results. (c) Cho *et al.* results. (d) AMEF results. (e) Yu *et al.* results. (f) Cai *et al.* results. (g) Yang *et al.* results. (h) Our results.

in Figure 3 (b-h). In addition, these methods can obtain some improvement of defogging the input images, improving global contrast, and preserving local detail information. Figure 3 (b) and (c) are the defogging results of the original images by DCP and Cho *et al.*, which don't sufficiently improve global contrast and some colour information is lost in the output images. The processed images look too dark, such as the tree area in image #3. The images processed by AMEF obtains a certain improvement in defogging, but the foreground colour of the processed image is bright, as shown in Figure 3 (d). The images acquired by Yu *et al.* are appeared in Figure 3 (e), the processed images can obtain reasonable defogging results, but overenhancement exhibits, and the whole images look too bright and the colour of some areas deviate from the background, such as the road area in images #3 and #4. Some areas of output images processed by Cai *et al.* and Yang *et al.* still look dark, as shown in Figure 3 (f) and (g). The output image by the proposed method exhibits a natural and clear defogging images, as indicated in Figure 3 (h).

Light haze indoor images and their defogging results obtained by different methods are indicated in Figure 4. The result of defogging by DCP method is displayed in Figure 4 (b), in which certain defogging effect can be obtained. Unfortunately, colour distortions are serious in the processed images, and the images look unnatural. Figure 4 (c) are defogging images by Cho *et al.*, in which overenhancements exist, for instance, table part in the images #6 and #8 is too bright. AMEF obtains limited improvement in defogging, so the output images look a little blurred and indistinct, as shown in Figure 4 (d). Figure 4 (e) is the result of the defogging images by Yu *et al.*. Similar to the processed light haze outdoor images, there are also existing overenhancements and some regions look too bright, such as the table area in images #6 and #8, and the floor area in image #7. Fog-free images by Cai *et al.* and Yang *et al.* are indicated in Figure 4 (f) and (g), it can be seen from observation that the two methods based on deep learning have achieved relatively good effects in defogging. However, image #7 still looks a little dim and the colour of some areas in images #8 and #9 deviate from the background. The proposed method can obtain a clearer image and the background colour of the image is closer to the original image compared with the other methods, as shown in Figure 4 (h).

Some defogging results for heavy haze outdoor images with different approaches are displayed in Figure 5. The background cannot be seen clearly in the original images due to the heavy fog. Therefore, the processing of heavy fog image is a challenging task. DCP and AMEF methods achieve limited improvement in defogging, as displayed in Figure 5 (b) and (d), the whole images are still dim and vague. Cho *et al.*'s method, in which the images #11, #12 and #13 can obtain certain defogging effects, but image #14 still looks blur, meanwhile, the background colour deviates from the original in image #15, as exhibited in Figure 5 (c). Yu *et al.*'s method causes the processed images existing overenhancement, and the whole images look unnatural in the defogged results in Figure 5 (e). Cai *et al.* and Yang *et al.* achieve limited improvement in defogging, as displayed in Figure 5 (f) and (g). Some images by Cai *et al.* and Yang *et al.*'s methods exist colour deviation from the original ones, for instance, image#15 in Figure 5 (f). Our advanced method can gain preferable image quality (Figure 5 (h)), which is manifested in the brightness improvement and fog removal.

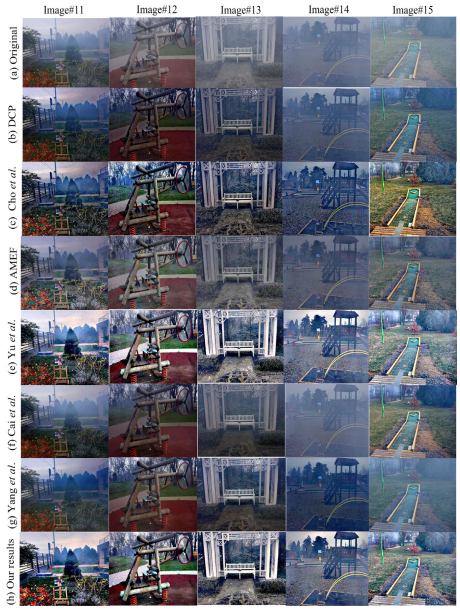

FIGURE 5. Comparisons of heavy haze outdoor images by various defogging algorithm. (a)Original images. (b)DCP results. (c) Cho *et al.* results. (d) AMEF results. (e) Yu *et al.* results. (f) Cai *et al.* results. (g) Yang *et al.* results. (h) Our results.

FIGURE 6. Comparisons of heavy haze outdoor images by various defogging algorithm. (a)Original images. (b)DCP results. (c) Cho *et al.* results. (d) AMEF results. (e) Yu *et al.* results. (f) Cai *et al.* results. (g) Yang *et al.* results. (h) Our results.

Heavy haze indoor images and their defogging versions achieved by various algorithms are illustrated in Figure 6. DCP method causes severe distortion in the background colour of the image, meanwhile, processed images #18 and #20 are too dim, as indicated in Figure 6 (b). Cho *et al.* and AMEF achieve limited defogging effects (Figure 6 (c) and (d)). Yu *et al.*'s method causes the images too bright to look unnatural due to the overenhancement of image contrast, which appear in Figure 6 (e). Cai *et al.* and Yang *et al.*'s approaches can defog the original im-ages (Figure 6 (e) and (f)); unfortunately, the output images look a little dim.

Some useful features of the image can be obtained by analyzing the image histogram, which can reflect some characteristics of the image. In our paper, the testing images have been divided into four types (light haze outdoor, light haze indoor, heavy haze outdoor and heavy haze indoor). From Figure 7, we can know that histograms of images in each type have different properties. The proposed method can outperform the other compared methods according to the objective analysis from Figures 3-6.

FIGURE 7. 20 testing images (top) and corresponding histograms (bottom).

B. OBJECTIVE EVALUATION

Further, to test the defogging performance of various comparison algorithms in an objective way, *PSNR* [66], *RMS* [67], *DE* [68], and *AG* [69] are employed for execution in comparison with some state-the-art algorithms, of which the descriptions are given in Section I.

PSNR is generally utilized to evaluate the quality achievement between the test images and reference images, which is based on the error between the corresponding pixels. It can measure the degree of image contrast enhancement. A large *PSNR* value denotes that the processed image has the smallest degradation by comparison with the original image [66].

Table 1 indicates some results of *PSNR* values with the investigated algorithms, as previously mentioned. The proposed algorithm can outperform the compared methods in *PSNR*, as displayed in Table 1.

RMS is commonly employed to measure the contrast of an image, in which a higher value represents better visibility of the processed image [60]. Some results are indicated in Table 2 for the *RMS* with the investigated

TABLE 1. Objective evaluation results in terms of *PSNR*.

Index	DCP	Cho et al.	AMEF	Yu et al.	Cai et al.	Yang et al.	Proposed
#1	36.18	30.17	32.99	42.22	48.30	31.40	**45.11**
#2	34.52	29.79	33.98	**65.55**	50.08	32.26	61.20
#3	39.10	27.75	22.47	52.03	45.28	39.26	**59.16**
#4	46.46	31.38	27.19	49.66	44.88	38.07	**51.18**
#5	33.36	30.25	38.53	**48.56**	42.47	32.61	37.74
#6	31.48	24.33	44.10	49.82	27.83	30.83	**50.94**
#7	28.86	24.96	48.70	46.36	29.05	32.81	**52.66**
#8	39.14	25.15	28.22	49.14	44.59	32.52	**52.92**
#9	44.64	27.66	30.95	**79.03**	38.18	36.63	63.83
#10	41.95	26.76	25.50	64.51	60.65	38.76	**68.96**
#11	51.73	28.22	20.29	32.12	57.99	58.18	**60.01**
#12	55.66	22.53	22.51	15.40	49.64	34.33	**56.22**
#13	58.43	27.86	26.19	14.89	**60.13**	33.33	57.00
#14	35.06	27.69	20.21	16.77	26.72	43.77	**39.80**
#15	27.16	18.38	29.72	14.18	29.90	21.85	**33.07**
#16	31.65	26.47	36.03	15.14	40.32	34.27	**40.01**
#17	48.39	28.83	28.45	17.00	46.11	36.81	**49.61**
#18	50.24	31.67	33.72	16.99	38.13	40.73	**52.12**
#19	26.04	19.70	28.06	13.22	28.65	23.69	**45.63**
#20	**49.64**	22.32	28.43	13.06	36.96	28.57	34.41

TABLE 2. Objective evaluation results in terms of *RMS*.

Index	DCP	Cho et al.	AMEF	Yu et al.	Cai et al.	Yang et al.	Proposed
#1	57.64	51.48	47.67	53.22	56.67	58.35	**59.57**
#2	76.19	78.12	69.10	85.55	75.46	72.26	**82.16**
#3	79.09	73.06	53.38	78.03	79.27	79.26	**81.71**
#4	55.36	**61.56**	47.60	59.66	51.33	52.21	60.44
#5	67.93	66.40	53.27	63.56	67.91	68.54	**71.57**
#6	62.69	62.35	68.25	59.82	60.22	67.63	70.28
#7	57.99	56.63	61.11	**60.36**	53.91	59.68	57.80
#8	50.74	61.91	45.07	63.14	50.23	56.11	**67.79**
#9	56.06	54.88	50.31	67.03	52.30	56.44	**69.41**
#10	42.32	48.50	35.48	69.51	45.74	43.61	**72.84**
#11	59.38	62.02	43.60	77.22	63.41	56.03	**80.43**
#12	34.83	57.96	36.31	65.49	34.47	40.15	**69.13**
#13	32.47	52.46	28.39	70.10	35.27	46.99	**71.85**
#14	36.62	34.78	28.93	41.40	39.46	40.79	**42.99**
#15	29.55	**49.80**	25.35	43.41	28.27	38.64	44.90
#16	42.87	56.05	33.04	67.92	38.44	49.23	**70.92**
#17	46.35	59.47	41.32	71.94	47.92	47.45	**70.45**
#18	44.89	45.33	39.18	51.81	51.07	53.11	**55.89**
#19	40.08	42.15	33.87	56.23	33.93	47.43	**56.97**
#20	31.98	48.72	29.60	54.43	31.03	46.05	**54.54**

methods, as previously mentioned. As indicated in Table 2, the Cho *et al.*'s method can obtain the best results for images #4 and #15, while Yu *et al.*'s has the best results for image #7. The developed algorithm performs best in all other test images. We discover that the best enhancement performances can be obtained by the proposed method, as displayed in Table 2.

The information richness in the image can be determined by Shannon entropy theory. The greater the entropy value of the image, the higher the information contained in the processed image will have [68]. Some results are given in Table 3 for *DE* [68] with the investigated approaches, as previously mentioned. The presented algorithm can outperform the compared methods in *DE*, as shown in Table 3.

TABLE 3. Objective evaluation results in terms of *DE*.

Index	DCP	Cho et al.	AMEF	Yu et al.	Cai et al.	Yang et al.	Proposed
#1	7.71	**7.88**	7.43	7.58	7.51	7.60	7.86
#2	7.38	7.68	7.72	7.45	7.69	7.39	**7.83**
#3	7.24	7.64	7.34	7.43	7.49	7.47	**7.71**
#4	7.29	7.66	7.42	7.68	7.28	7.22	**7.77**
#5	7.21	7.22	6.86	7.03	6.75	7.04	**7.24**
#6	7.16	6.73	7.14	6.58	6.96	7.18	**7.23**
#7	6.98	6.81	7.03	6.23	6.61	6.42	**7.26**
#8	7.46	7.69	7.38	7.74	7.56	7.63	**7.75**
#9	7.06	7.43	7.29	7.41	7.39	7.15	**7.72**
#10	7.22	7.52	7.00	**7.78**	7.32	7.22	7.77
#11	7.67	7.81	7.43	7.68	7.74	7.44	**7.86**
#12	6.88	7.62	7.20	7.82	6.96	7.06	**7.79**
#13	6.97	7.64	6.83	7.85	7.08	7.35	**7.78**
#14	6.34	7.07	5.92	7.14	6.14	6.59	**7.23**
#15	6.80	**7.56**	6.60	7.36	6.60	7.19	7.41
#16	7.33	7.76	7.01	7.74	7.12	7.37	**7.78**
#17	7.17	7.62	7.30	7.71	7.40	7.17	**7.65**
#18	7.11	7.33	7.06	7.47	7.59	7.29	**7.66**
#19	6.74	7.14	6.77	7.38	6.39	7.15	**7.48**
#20	6.31	7.31	6.53	7.49	6.57	7.04	**7.44**

The average gradient (*AG*) is the mean value of the gray change rate, which is commonly used to represent the image clarity [69]. It is caused by the obvious difference of the gray level near the edge of the image or the shadow line. The higher the value of *AG*, the clearer the output image.

TABLE 4. Objective evaluation results in terms of *AG*.

Index	DCP	Cho et al.	AMEF	Yu et al.	Cai et al.	Yang et al.	Proposed
#1	20.18	**25.22**	18.35	21.40	12.97	15.08	21.28
#2	13.41	18.97	14.70	18.82	10.60	9.95	**19.78**
#3	7.99	13.53	9.68	14.14	6.27	6.32	**14.72**
#4	17.76	26.87	20.45	25.98	14.33	15.05	**27.23**
#5	8.78	**9.79**	6.71	8.48	5.76	6.87	8.62
#6	5.83	6.17	5.16	4.47	4.15	5.00	**6.35**
#7	4.58	5.40	3.91	4.30	3.52	3.83	**5.65**
#8	8.30	10.22	7.43	9.91	6.40	7.28	**10.59**
#9	5.66	6.88	4.04	**6.81**	3.31	3.78	6.36
#10	4.12	7.29	4.19	7.62	3.15	3.99	**7.86**
#11	8.18	14.64	12.39	15.80	6.67	7.13	**18.75**
#12	8.94	15.20	10.14	15.22	6.72	8.79	**15.88**
#13	8.46	16.09	9.04	18.85	5.35	9.21	**18.02**
#14	6.85	11.38	9.10	11.65	5.44	6.89	**12.29**
#15	9.42	17.10	10.13	17.87	6.91	11.38	**18.03**
#16	6.01	8.75	5.01	9.32	4.44	6.04	**9.42**
#17	6.84	9.33	6.38	9.28	4.81	5.46	**9.30**
#18	4.34	5.88	4.10	6.25	2.60	3.42	**6.03**
#19	3.66	5.88	3.32	6.05	2.68	3.40	**5.99**
#20	4.70	7.20	4.36	7.22	3.66	5.25	**7.68**

Some results are given in Table 4 for *AG* with the investigated methods, as previously mentioned. We determine from Table 4 that the proposed algorithm creates a larger *AG* value in most of the cases and its performance is the best compared with the other methods.

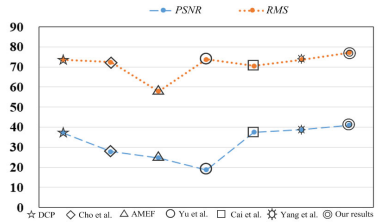

(a) Quantitative analysis results (average) of 500 test images: *PSNR* and *RMS*

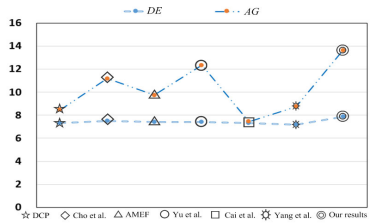

(b) Quantitative analysis results (average) of 500 test images: *DE* and *AG*.

FIGURE 8. Quantitative analysis of four evaluation functions.

Compared with other six algorithms, the performance of the proposed method for most of the twenty test images is satisfactory. Therefore, in addition to the twenty test images, the four objective evaluation functions (i.e., *PSNR* [66], *RMS* [67], *DE* [68], and *AG* [69]) are utilized on the 500 randomly selected test images from public datasets to further verify the performance and capability of the proposed method. Figures 8 (a) and (b) show the average values of the quantitative analyses for the random selection of 500 images.

From Figures IV-B (a) and (b), we can know that the proposed algorithm has outstanding performance compared with other state-of-the-art algorithms. On average, the images processed by the proposed method contain the highest amount of information. Our method has the highest *RMS* value, with an average of 77.18 for 500 randomly selected test images. It means that our method can obtain the best effect of maintaining the information details and richness in the processed images. The largest average value of *PSNR* (40.96) is also got by our method, which indicates that the present algorithm outperforms all other methods on image contrast enhancement. The proposed algorithm outperforms all other methods and can obtain the largest *DE* and *AG* values, which means that the processed images have a clearer appearance with minimum artefacts according to the comparison with others.

To analyse the performance of computational time, 500 test images with the size of 640 × 480 are further employed. All the experiments are performed on a Windows 10 Pro system with 2.4 GHz CPU and 4 GB RAM. The algorithms are carried out on MATLAB 2018a using the default parameters by the respective authors' suggestions.

The results in Table 5 show that the execution time of the proposed algorithm is comparable with other histogram-division-based algorithms. The method by Yu *et al.* takes a much longer time than others. Average processing time of the proposed method can outperform those of most of the compared methods, and therefore it is suitable for real-time applications.

TABLE 5. Average running time (*s*).

DCP	Cho et al.	AMEF	Yu et al.	Cai et al.	Yang et al.	Proposed
2.07	1.32	1.61	5.36	3.23	3.07	1.28

The performance of the proposed method of this study is acceptable according to the results of the experiments.

V. CONCLUSION

In this paper, to remove haze of hazy images, a combining algorithm is introduced. In the algorithm, ambient illumination is predicted by logarithmic guide filtering. Then, to obtain the value of the transmission $t(x)$, first, a multi-channel prior method is proposed, which contains two models with two parameters and the values of the two parameters can be self-adaptively calculated. Then, a weight factor self-adaptively calculated is presented in the equation, which is employed to reckon the transmission $t(x)$. At last, a well-quality dehazing image is obtained. In the experiment section, which is executed in four types(light haze outdoor/indoor, heavy haze outdoor/indoor), it is obtained that (1) Experiments on the selected 20 testing images (divided into four types: light haze outdoor images; light haze indoor images; heavy haze outdoor images; heavy haze indoor images) show that our method can outperform the others both in the subjective and objective evaluations; (2) *PSNR*, *RMS*, *DE*, and *AG* values on 500 randomly selected testing images demonstrate that the performance and capability of our method have better robustness; (3) The average running time of the presented method is acceptable by analyzing the performance of computational time.

As a future research, combining multi-fusion methods with logarithmic guide filtering can be utilized to address other image processing research areas.

ACKNOWLEDGMENT

The authors are grateful to anonymous referees for their helpful comments and suggestions, which have led to much improvement of the article.

AUTHOR CONTRIBUTIONS

Yuanyang Zou implemented the core algorithm and drafted the manuscript. Liyun Zhuang reviewed and edited the manuscript. All authors discussed the results and implications, commented on the manuscript at all stages, and approved the final version.

CONFLICTS OF INTEREST

All authors declare that there are no conflicts of interest regarding the publication of this paper.

REFERENCES

[1] H. Zhang, V. Sindagi, and V. M. Patel, "Multi-scale single image dehazing using perceptual pyramid deep network," in *Proc. IEEE/CVF Conf. Comput. Vis. Pattern Recognit. Workshops (CVPRW)*, Jun. 2018, pp. 902–911.

[2] J. S. Laine, "Adapting softcopy color reproduction to ambient illumination," *J. Soc. Inf. Display*, vol. 11, no. 2, pp. 359–369, Jun. 2012.

[3] J. A. Brennan, P. Brennan, and T. M. Haygood, "Ambient lighting in the reading room: Theoretical concepts and practical outcomes," *Current Med. Imag. Rev.*, vol. 6, no. 3, pp. 156–164, Aug. 2010.

[4] C.-C. Lin and K.-C. Huang, "Effects of ambient illumination conditions and background color on visual performance with TFT-LCD screens," *Displays*, vol. 34, no. 4, pp. 276–282, Oct. 2013.

[5] R. Gong, H. Xu, Q. Wang, Z. Wang, and H. Li, "Investigation of perceptual attributes for mobile display image quality," *Opt. Eng.*, vol. 52, no. 8, Aug. 2013, Art. no. 083104.

[6] X. Jin, P. Deng, X. Li, K. Zhang, X. Li, Q. Zhou, S. Xie, and X. Fang, "Sun-sky model estimation from outdoor images," *J. Ambient Intell. Humanized Comput.*, vol. 11, no. 8, pp. 1–12, Aug. 2020.

[7] S.-M. Woo, S.-H. Lee, J.-S. Yoo, and J.-O. Kim, "Improving color constancy in an ambient light environment using the phong reflection model," *IEEE Trans. Image Process.*, vol. 27, no. 4, pp. 1862–1877, Apr. 2018.

[8] J. Zhang, Y. Cao, and Z. Wang, "Nighttime haze removal based on a new imaging model," in *Proc. IEEE Int. Conf. Image Process. (ICIP)*, Oct. 2014, pp. 4557–4561.

[9] W. Lou, Y. Li, G. Yang, C. Chen, H. Yang, and T. Yu, "Integrating haze density features for fast nighttime image dehazing," *IEEE Access*, vol. 8, pp. 113318–113330, 2020.

[10] M. Li, J. Liu, W. Yang, X. Sun, and Z. Guo, "Structure-revealing low-light image enhancement via robust retinex model," *IEEE Trans. Image Process.*, vol. 27, no. 6, pp. 2828–2841, Jun. 2018.

[11] H. Koschmieder, *Theorie der Horizontalen Sichtweite: Kontrast und Sichtweite*. Munich, Germany: Keim & Nemnich, 1925.

[12] K. He, J. Sun, and X. Tang, "Single image haze removal using dark channel prior," *IEEE Trans. Pattern Anal. Mach. Intell.*, vol. 33, no. 12, pp. 2341–2353, Dec. 2011.

[13] S. G. Narasimhan and S. K. Nayar, "Contrast restoration of weather degraded images," *IEEE Trans. Pattern Anal. Mach. Intell.*, vol. 25, no. 6, pp. 713–724, Jun. 2003.

[14] R. Fattal, "Single image dehazing," *ACM Trans. Graph.*, vol. 27, no. 3, pp. 1–9, Aug. 2008.

[15] R. T. Tan, "Visibility in bad weather from a single image," in *Proc. IEEE Conf. Comput. Vis. Pattern Recognit.*, Jun. 2008, pp. 1–8.

[16] K. Nishino, L. Kratz, and S. Lombardi, "Bayesian defogging," *Int. J. Comput. Vis.*, vol. 98, no. 3, pp. 263–278, Jul. 2012.

[17] J.-P. Tarel and N. Hautiere, "Fast visibility restoration from a single color or gray level image," in *Proc. IEEE 12th Int. Conf. Comput. Vis.*, Sep. 2009, pp. 2201–2208.

[18] Q. Zhu, J. Mai, and L. Shao, "A fast single image haze removal algorithm using color attenuation prior," *IEEE Trans. Image Process.*, vol. 24, no. 11, pp. 3522–3533, Nov. 2015.

[19] R. Fattal, "Dehazing using color-lines," *ACM Trans. Graph.*, vol. 34, no. 1, pp. 1–14, Dec. 2014.

[20] X. Ma, Y. Hong, and Y. Song, "Super resolution land cover mapping of hyperspectral images using the deep image prior-based approach," *Int. J. Remote Sens.*, vol. 41, no. 7, pp. 2818–2834, Apr. 2020.

[21] D. Singh and V. Kumar, "Image dehazing using Moore neighborhood-based gradient profile prior," *Signal Process., Image Commun.*, vol. 70, pp. 131–144, Feb. 2019.

[22] T. M. Bui and W. Kim, "Single image dehazing using color ellipsoid prior," *IEEE Trans. Image Process.*, vol. 27, no. 2, pp. 999–1009, Feb. 2018.

[23] M. Kaur, D. Singh, V. Kumar, and K. Sun, "Color image dehazing using gradient channel prior and guided L_0 filter," *Inf. Sci.*, vol. 521, pp. 326–342, Jun. 2020.

[24] H. Khan, M. Sharif, N. Bibi, M. Usman, S. A. Haider, S. Zainab, J. H. Shah, Y. Bashir, and N. Muhammad, "Localization of radiance transformation for image dehazing in wavelet domain," *Neurocomputing*, vol. 381, pp. 141–151, Mar. 2020.

[25] R. M. Yousaf, H. A. Habib, Z. Mehmood, and M. Bilal, "Image dehazing based on dark channel spatial stimuli gradient model and image morphology," *J. Ambient Intell. Humanized Comput.*, vol. 11, no. 10, pp. 1–13. Oct. 2020.

[26] K. He, J. Sun, and X. Tang, "Guided image filtering," in *Proc. Eur. Conf. Comput. Vis.*, Sep. 2010, pp. 1–14.

[27] K. Tang, J. Yang, and J. Wang, "Investigating haze-relevant features in a learning framework for image dehazing," in *Proc. IEEE Conf. Comput. Vis. Pattern Recognit.*, Jun. 2014, pp. 2995–3000.

[28] B. Cai, X. Xu, K. Jia, C. Qing, and D. Tao, "DehazeNet: An end-to-end system for single image haze removal," *IEEE Trans. Image Process.*, vol. 25, no. 11, pp. 5187–5198, Nov. 2016.

[29] B. Li, X. Peng, Z. Wang, J. Xu, and D. Feng, "AOD-net: All-in-one dehazing network," in *Proc. IEEE Int. Conf. Comput. Vis. (ICCV)*, Oct. 2017, pp. 4770–4778.

[30] D. Huang, K. Chen, J. Lu, and W. Wang, "Single image dehazing based on deep neural network," in *Proc. Int. Conf. Comput. Netw., Electron. Autom. (ICCNEA)*, Sep. 2017, pp. 294–299.

[31] Y. Song, J. Li, X. Wang, and X. Chen, "Single image dehazing using ranking convolutional neural network," *IEEE Trans. Multimedia*, vol. 20, no. 6, pp. 1548–1560, Jun. 2018.

[32] C. Li, C. Guo, J. Guo, P. Han, H. Fu, and R. Cong, "PDR-net: Perception-inspired single image dehazing network with refinement," *IEEE Trans. Multimedia*, vol. 22, no. 3, pp. 704–716, Mar. 2020.

[33] Z. Li, B. Gui, T. Zhen, and Y. Zhu, "Grain depot image dehazing via quadtree decomposition and convolutional neural networks," *Alexandria Eng. J.*, vol. 59, no. 3, pp. 1463–1472, Jun. 2020.

[34] A. Khatun, M. R. Haque, R. Basri, and M. S. Uddin, "Single image dehazing: An analysis on generative adversarial network," *J. Comput. Commun.*, vol. 8, no. 4, 2020, Art. no. 99931.

[35] H. Zhang and V. M. Patel, "Densely connected pyramid dehazing network," in *Proc. IEEE/CVF Conf. Comput. Vis. Pattern Recognit.*, Jun. 2018, pp. 3194–3203.

[36] D. Engin, A. Genc, and H. K. Ekenel, "Cycle-dehaze: Enhanced CycleGAN for single image dehazing," in *Proc. IEEE/CVF Conf. Comput. Vis. Pattern Recognit. Workshops (CVPRW)*, Jun. 2018, pp. 825–833.

[37] D. Yang and J. Sun, "Proximal dehaze-net: A prior learning-based deep network for single image dehazing," in *Proc. Eur. Conf. Comput. Vis. (ECCV)*, Sep. 2018, pp. 702–717.

[38] A. Wang, W. Wang, J. Liu, and N. Gu, "AIPNet: Image-to-image single image dehazing with atmospheric illumination prior," *IEEE Trans. Image Process.*, vol. 28, no. 1, pp. 381–393, Jan. 2019.

[39] R. Li, J. Pan, M. He, Z. Li, and J. Tang, "Task-oriented network for image dehazing," *IEEE Trans. Image Process.*, vol. 29, no. 5, pp. 6523–6534, May 2020.

[40] J. Park, D. K. Han, and H. Ko, "Fusion of heterogeneous adversarial networks for single image dehazing," *IEEE Trans. Image Process.*, vol. 29, no. 2, pp. 4721–4732, Feb. 2020.

[41] B. Li, Y. Gou, J. Z. Liu, H. Zhu, J. T. Zhou, and X. Peng, "Zero-shot image dehazing," *IEEE Trans. Image Process.*, vol. 29, no. 8, pp. 8457–8466, Aug. 2020.

[42] C. Wang, Z. Li, J. Wu, H. Fan, G. Xiao, and H. Zhang, "Deep residual haze network for image dehazing and deraining," *IEEE Access*, vol. 8, pp. 9488–9500, 2020.

[43] K. Metwaly, X. Li, T. Guo, and V. Monga, "NonLocal channel attention for NonHomogeneous image dehazing," in *Proc. IEEE/CVF Conf. Comput. Vis. Pattern Recognit. Workshops (CVPRW)*, Jun. 2020, pp. 452–453.

[44] C. O. Ancuti and C. Ancuti, "Single image dehazing by multi-scale fusion," *IEEE Trans. Image Process.*, vol. 22, no. 8, pp. 3271–3282, Aug. 2013.

[45] A. Galdran, J. Vazquez-Corral, D. Pardo, and M. Bertalmío, "Fusion-based variational image dehazing," *IEEE Signal Process. Lett.*, vol. 24, no. 2, pp. 151–155, Feb. 2017.

[46] Y. Gao, Y. Su, Q. Li, and J. Li, "Single fog image restoration with multi-focus image fusion," *J. Vis. Commun. Image Represent.*, vol. 55, pp. 586–595, Aug. 2018.

[47] A. Galdran, "Image dehazing by artificial multiple-exposure image fusion," *Signal Process.*, vol. 149, pp. 135–147, Aug. 2018.

[48] Y. Gao, Y. Su, Q. Li, H. Li, and J. Li, "Single image dehazing via self-constructing image fusion," *Signal Process.*, vol. 167, Feb. 2020, Art. no. 107284.

[49] C. Chen, S. Li, Y. Wang, H. Qin, and A. Hao, "Video saliency detection via spatial-temporal fusion and low-rank coherency diffusion," *IEEE Trans. Image Process.*, vol. 26, no. 7, pp. 3156–3170, Jul. 2017.

[50] C. Chen, J. Wei, C. Peng, W. Zhang, and H. Qin, "Improved saliency detection in RGB-D images using two-phase depth estimation and selective deep fusion," *IEEE Trans. Image Process.*, vol. 29, pp. 4296–4307, Jan. 2020.

[51] Z. Zhu, H. Wei, G. Hu, Y. Li, G. Qi, and N. Mazur, "A novel fast single image dehazing algorithm based on artificial multiexposure image fusion," *IEEE Trans. Instrum. Meas.*, vol. 70, 2021. Art. no. 5001523.

[52] M. Zheng, G. Qi, Z. Zhu, Y. Li, H. Wei, and Y. Liu, "Image dehazing by an artificial image fusion method based on adaptive structure decomposition," *IEEE Sensors J.*, vol. 20, no. 14, pp. 8062–8072, Jul. 2020.
[53] S. C. Agrawal and A. S. Jalal, "Visibility improvement of hazy image using fusion of multiple exposure images," in *Smart Innovations in Communication and Computational Sciences*. Singapore: Springer, Aug. 2020, pp. 321–332.
[54] S. Hong, M. Kim, and M. G. Kang, "Single image dehazing via atmospheric scattering model-based image fusion," *Signal Process.*, vol. 178, Jan. 2021, Art. no. 107798.
[55] Y. Cho, J. Jeong, and A. Kim, "Model assisted multi-band fusion for single image enhancement and applications to robot vision," *IEEE Robot. Autom. Letters.*, vol. 3, no. 4, pp. 2822–2829, Jun. 2018.
[56] T. Yu, K. Song, P. Miao, G. Yang, H. Yang, and C. Chen, "Nighttime single image dehazing via pixel-wise alpha blending," *IEEE Access*, vol. 7, pp. 114619–114630, 2019.
[57] E. H. Land, "The retinex theory of color vision," *Sci. Amer.*, vol. 237, no. 6, pp. 108–129, Dec. 1977.
[58] Y. B. Yu, N. J. Yang, C. Y. Yang, and N. Tashi, "Memristor bridge-based low pass filter for image processing," *J. Syst. Eng. Electron.*, vol. 30, no. 3, pp. 448–455, Jun. 2019.
[59] Z. Rahman, D. J. Jobson, and G. A. Woodell, "Multi-scale retinex for color image enhancement," in *Proc. 3rd IEEE Int. Conf. Image Process.*, vol. 3, Sep. 1996, pp. 1003–1006.
[60] R. Marazzato and A. C. Sparavigna, "Retinex filtering of foggy images: Generation of a bulk set with selection and ranking," Sep. 2015, *arXiv:1509.08715*. [Online]. Available: http://arxiv.org/abs/1509.08715
[61] Z. Sun, B. Han, J. Li, J. Zhang, and X. Gao, "Weighted guided image filtering with steering kernel," *IEEE Trans. Image Process.*, vol. 29, no. 7, pp. 500–508, Jul. 2020.
[62] A. Golts, D. Freedman, and M. Elad, "Unsupervised single image dehazing using dark channel prior loss," *IEEE Trans. Image Process.*, vol. 29, pp. 2692–2701, Nov. 2019.
[63] C. O. Ancuti, C. Ancuti, R. Timofte, and C. De Vleeschouwer, "O-HAZE: A dehazing benchmark with real hazy and haze-free outdoor images," in *Proc. IEEE/CVF Conf. Comput. Vis. Pattern Recognit. Workshops (CVPRW)*, Jun. 2018, pp. 620–631.
[64] C. O. Ancuti, C. Ancuti, R. Timofte, and C. D. Vleeschouwer, "I-HAZE: A dehazing benchmark with real hazy and haze-free indoor images," in *Proc. Int. Conf. Adv. Concepts Intell. Vis. Syst.*, Jun. 2018, pp. 867–875.
[65] C. O. Ancuti, C. Ancuti, and R. Timofte, "NH-HAZE: An image dehazing benchmark with non-homogeneous hazy and haze-free images," in *Proc. IEEE/CVF Conf. Comput. Vis. Pattern Recognit. Workshops (CVPRW)*, Jun. 2020, pp. 1798–1805.
[66] Y. Huang, B. Niu, H. Guan, and S. Zhang, "Enhancing image watermarking with adaptive embedding parameter and PSNR guarantee," *IEEE Trans. Multimedia*, vol. 21, no. 10, pp. 2447–2460, Oct. 2019.
[67] K. Jacobs, C. Loscos, and G. Ward, "Automatic high-dynamic range image generation for dynamic scenes," *IEEE Comput. Graph. Appl.*, vol. 28, no. 2, pp. 84–93, Mar. 2008.
[68] J. Shin, M. Kim, J. Paik, and S. Lee, "Radiance–reflectance combined optimization and structure-guided ℓ_0-norm for single image dehazing," *IEEE Trans. Multimedia*, vol. 22, no. 1, pp. 30–44, Jan. 2020.
[69] D. Singh, V. Kumar, and M. Kaur, "Single image dehazing using gradient channel prior," *Int. J. Speech Technol.*, vol. 49, no. 12, pp. 4276–4293, Jun. 2019.

YUANYANG ZOU received the B.S. degree in business management from the Fujian University of Technology, in 2006, the M.S. degree in applied mathematics from Jinan University, in 2015, and the Ph.D. degree in management science and engineering from Shanghai University, in 2018. He is currently working with the School of Business Administration, Hubei University of Economics, Wuhan, China. His research interests include traffic optimization and optimal control.

YINGSHUANG MA received the M.S. degree from Yangtze University, Hubei, China, in 2007, and the Ph.D. degree in management science and engineering from Shanghai University, Shanghai, China. He is currently an Associate Professor with the Faculty of Business School, Huanggang Normal University. His research interests include neuro management and decision neuroscience.

LIYUN ZHUANG received the M.S. degree from the China University of Mining and Technology, Xuzhou, China, in 2009, and the Ph.D. degree in communication and information system from Shanghai University, Shanghai, China. He is currently a Lecturer with the Faculty of Electronic and Information Engineering, Huaiyin Institute of Technology. His research interests include computer vision and pattern recognition.

GUOXIN WANG received the B.S. degree in mathematics from Nanyang Normal University, in 2004, the M.S. degree in operations research and cybernetics and the Ph.D. degree in management science and engineering from Shanghai University in 2007 and 2018, respectively. She is currently working with the School of Mathematics and Statistics, Nanyang Institute of Technology, Nanyang, China. Her research interests include mathematical optimization and stochastic optimization.